Special feature: Bioresorbable scaffolds

Preclinical evaluation of a thin-strut bioresorbable scaffold (ArterioSorb)

Yuki Katagiri[1], MD; Ryo Torii[2], PhD; Kuniaki Takahashi[1], MD; Erhan Tenekecioglu[3], MD; Taku Asano[1], MD; Ply Chichareon[1], MD; Mariusz Tomaniak[3,4], MD; Jan J. Piek[1], MD, PhD; Joanna J. Wykrzykowska[1], MD, PhD; Nial Bullett[5], PhD; Naveed Ahmed[5], PhD; Kadem Al-Lamee[5], PhD; Rasha Al-Lamee[6], MD, PhD; Guy Leclerc[7], MD; Pieter Kitslaar[8], MSc; Jouke Dijkstra[8], PhD; Johan H.C. Reiber[8], PhD; Eric K.W. Poon[9], PhD; Christos V. Bourantas[10,11,12], MD, PhD; Frank Gijsen[13], PhD; Patrick W. Serruys[14]*, MD, PhD; Yoshinobu Onuma[14], MD, PhD

1. Amsterdam University Medical Centre, University of Amsterdam, Amsterdam, the Netherlands; 2. Department of Mechanical Engineering, University College London, London, United Kingdom; 3. Department of Interventional Cardiology, Thoraxcenter, Erasmus Medical Center, Rotterdam, the Netherlands; 4. First Department of Cardiology, Medical University of Warsaw, Warsaw, Poland; 5. Arterius Ltd, Leeds, United Kingdom; 6. Imperial College London, London, United Kingdom; 7. AccelLAB Inc., Boisbriand, QC, Canada; 8. LKEB-Division of Image Processing, Department of Radiology, Leiden University Medical Center, Leiden, the Netherlands; 9. Department of Mechanical Engineering, Melbourne School of Engineering, University of Melbourne, Parkville, Australia; 10. Institute of Cardiovascular Sciences, University College London, London, United Kingdom; 11. Department of Cardiology, Barts Heart Centre, London, United Kingdom; 12. School of Medicine and Dentistry, Queen Mary University of London, London, United Kingdom; 13. Department of Biomedical Engineering, Thoraxcenter, Erasmus Medical Center, Rotterdam, the Netherlands; 14. Department of Cardiology, National University of Ireland, Galway (NUIG), Galway, Ireland

GUEST EDITOR: Alec Vahanian, MD, PhD; *Department of Cardiology, Hôpital Bichat-Claude Bernard, and University Paris VII, Paris, France*

This paper also includes supplementary data published online at: https://eurointervention.pcronline.com/doi/10.4244/EIJ-D-18-01190

KEYWORDS

- bioresorbable scaffolds
- drug-eluting stent
- optical coherence tomography
- QCA

Abstract

Aims: The aim of this study was to assess the acute performance of the 95 µm ArterioSorb oriented poly L-lactic acid (PLLA) scaffold in comparison with the XIENCE metallic drug-eluting stent (DES) in porcine coronary arteries.

Methods and results: In 15 non-atherosclerotic Yucatan mini pigs, the ArterioSorb (3.0/14 mm) and XIENCE (3.0/15 mm) were implanted in 25 and 15 vessels, respectively. Acute performance was evaluated by using quantitative coronary angiography (QCA) and optical coherence tomography (OCT). Following three-dimensional reconstruction of the coronary arteries, endothelial shear stress (ESS) was quantified using non-Newtonian steady-flow simulation. Acute recoil measured by QCA was comparable in the two arms. Post-procedural flow and scaffold/stent area by OCT did not differ between the two devices. ESS post procedure was comparable between ArterioSorb and XIENCE (2.21±1.97 vs 2.25±1.71 Pa, p=0.314).

Conclusions: Acute recoil, luminal dimensions and ESS in the ArterioSorb oriented PLLA scaffold with thin struts of 95 µm were comparable to those in the XIENCE metallic DES.

**Corresponding author: Department of Cardiology, National University of Ireland, University Road, Galway, H91 TK33, Ireland. E-mail: patrick.w.j.c.serruys@gmail.com*

SUBMITTED ON 17/12/2018 - REVISION RECEIVED ON 1st 21/04/2019 / 2nd 08/06/2019 - ACCEPTED ON 03/07/2019

Abbreviations

BRS	bioresorbable scaffold
CFD	computational fluid dynamics
DES	drug-eluting stent
ESS	endothelial shear stress
OCT	optical coherence tomography
PDLLA	poly (D, L-lactic acid)
PLLA	poly L-lactic acid
QCA	quantitative coronary angiography
SB	side branch
ST	scaffold thrombosis

Introduction

Bioresorbable scaffolds (BRS) were developed with the hope that they would overcome the long-term complications observed with metallic drug-eluting stents (DES) including delayed vessel healing, hypersensitivity reactions, restenosis, and neoatherosclerosis with the risk of repeat intervention and stent thrombosis (ST). However, the Absorb™ (Abbott Vascular, Santa Clara, CA, USA), the most investigated BRS, was shown to have an increased risk of target lesion failure in comparison with a contemporary everolimus-eluting metallic DES (XIENCE; Abbott Vascular)[1].

The ArterioSorb™ scaffold (Arterius Ltd, Leeds, United Kingdom) was developed as a second-generation BRS using a patented die-drawing processing technique of poly L-lactic acid (PLLA) that results in improved radial strength, allowing reduced strut thickness. This results in a low crossing profile and is likely to reduce the occurrence of in-device thrombosis caused by bulky struts disrupting the arterial blood flow (i.e., endothelial shear stress [ESS]).

The aim of this study was *in vivo* assessment of angiographic and optical coherence tomography (OCT) results, and ESS distribution following ArterioSorb PLLA scaffold and XIENCE metallic DES implantation in the coronary arteries of Yucatan mini pigs.

Methods

STUDY DEVICES

The ArterioSorb scaffold comprises an oriented PLLA backbone with a strut thickness of 95 µm, coated with a layer of poly (D, L-lactic acid) (PDLLA) eluting rapamycin (1.45 µg/mm^2) **(Supplementary Figure 1)**. The ArterioSorb is manufactured using melt processing (extrusion) and die-drawing (solid-phase orientation) techniques. The strut width of the ArterioSorb is 170 µm.

The control everolimus-eluting durable polymer XIENCE stent is a cobalt-chromium alloy device with a strut thickness of 89 µm. The strut width of the XIENCE stent is 81.3 µm.

The *in vitro* study demonstrated that the mechanical properties of the ArterioSorb were equivalent to the metallic DES **(Supplementary Appendix 1**[2]**, Supplementary Figure 2, Supplementary Figure 3)**.

STUDY DESIGN

Fifteen non-atherosclerotic Yucatan mini pigs were included. The ArterioSorb (3.0 mm diameter × 14 mm length) and the XIENCE (3.0 mm diameter × 15 mm length) were used. When possible, an ArterioSorb or XIENCE was implanted in the three coronary arteries (right coronary artery, left anterior descending artery, and left circumflex artery), depending on the suitability of the vessel diameter measured by preprocedural angiography and OCT. The types of device implanted were balanced among the three coronary arteries. A maximum of four devices per animal were implanted. Y. Onuma attended the experiments. The protocol was reviewed and approved by the Institutional Animal Care and Use Committee of the testing facility (AccelLAB Inc., Boisbriand, Quebec, Canada). The review ensured compliance with Canadian Council on Animal Care regulations. The testing facility is accredited by the Association for Assessment and Accreditation of Laboratory Animal Care (AAALAC) and the Canadian Council on Animal Care (CCAC).

PROCEDURE DETAILS

A scaffold/stent was deployed in a segment of coronary artery free from side branches, whenever possible. Post-dilatation using a non-compliant balloon catheter was performed to achieve a targeted balloon-to-artery ratio of 1.1:1 and to ensure good apposition and embedment of the scaffold/stent struts under OCT guidance.

DATA ACQUISITION AND QCA/OCT ANALYSIS

The specific details of the data acquisition and quantitative coronary angiography (QCA) and OCT analyses are provided in **Supplementary Appendix 2**[3-5].

SHEAR STRESS ANALYSIS

The detailed methods of three-dimensional reconstruction of the coronary artery and subsequent computational fluid dynamics (CFD) analysis are included in **Supplementary Appendix 3**[6-13].

STATISTICAL ANALYSIS

The statistical analysis methods are described in **Supplementary Appendix 4**[13].

Results

PROCEDURAL CHARACTERISTICS

Procedural characteristics are shown in **Supplementary Table 1**. Maximal pressure during device implantation or post-dilatation was not statistically different between the ArterioSorb and XIENCE devices. Post-dilatation was performed in all scaffolds in the ArterioSorb arm, whereas in the XIENCE arm 80% of stents were post-dilated (p=0.046).

ACUTE PERFORMANCE

Periprocedural QCA measurements are shown in **Supplementary Table 2**. Device balloon-artery ratio as well as post-dilatation balloon-artery ratio were comparable between the two arms. Post-procedural mean or minimum lumen diameter was similar in the two arms. **Figure 1** shows serial changes in mean lumen and balloon diameter during the procedure. Absolute recoil after device deployment and the one after post-dilatation were comparable between ArterioSorb and XIENCE.

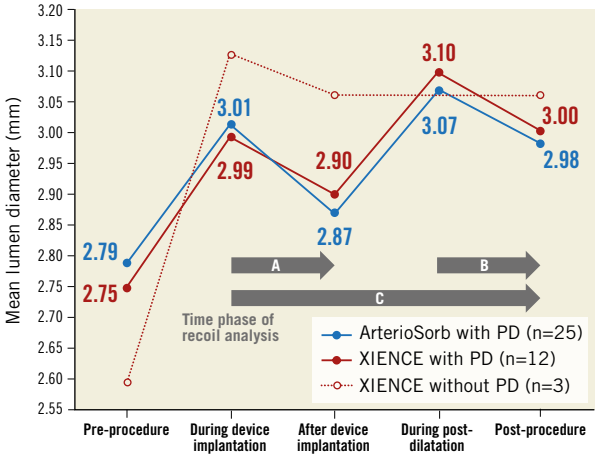

	ArterioSorb	XIENCE	*p*-value
Immediately after device deployment (A)	N=25	N=15	
Absolute recoil (mm)	0.14±0.22	0.09±0.15	0.388
Relative recoil (%)	4.69±7.38	2.70±4.52	0.367
From PD to post-procedure (B)	N=25	N=12	
Absolute recoil (mm)	0.09±0.17	0.10±0.16	0.931
Relative recoil (%)	2.81±5.52	3.03±5.21	0.907
Global recoil (C)	N=25	N=12	
Absolute recoil (mm)	0.03±0.27	−0.01±0.18	0.636
Relative recoil (%)	0.55±8.27	−0.46±5.64	0.705

Figure 1. *Recoil assessment by quantitative coronary angiography during procedure. The graph lines show serial changes in mean lumen diameter in device segments. PD: post-dilatation*

Table 1 shows that quantitative OCT results post procedure did not differ significantly between ArterioSorb and XIENCE.

SHEAR STRESS COMPARISON BETWEEN ARTERIOSORB AND XIENCE

Supplementary Figure 4 shows a study flow chart for the CFD analysis. There were 10 scaffolds and five metallic stents excluded from the shear stress analysis due to technical reasons (i.e., absence of landmarks) in ArterioSorb and XIENCE, respectively. Finally, 134,856 five-degree sectors in 15 ArterioSorb scaffolds and 104,328 sectors in 10 XIENCE stents were included in the statistical analysis. **Figure 2** shows cumulative frequency curves of ESS in five-degree sectors in cross-sections. ESS post procedure was comparable between ArterioSorb and XIENCE (2.21±1.97 vs 2.25±1.71 Pa, p=0.314). In contrast, relative area exposed to low ESS (<1 Pa) was larger in ArterioSorb than in XIENCE, although this did not reach statistical significance **(Table 2)**.

Table 1. Results of optical coherence tomography post procedure.

	ArterioSorb (n=25)	XIENCE (n=15)	*p*-value
Reference lumen area, mm^2	7.13±1.00	7.17±1.69	0.929
Mean flow area, mm^2	7.93±0.85	7.91±0.94	0.953
Minimal flow area, mm^2	6.94±0.80	6.75±0.77	0.446
Mean abluminal scaffold/stent area, mm^2	8.87±0.92	9.01±1.00	0.655
Mean endoluminal scaffold/stent area, mm^2	8.07±0.88	8.11±0.95	0.880
Minimal abluminal scaffold/stent area, mm^2	7.83±0.87	7.81±0.81	0.929
Minimal endoluminal scaffold/stent area, mm^2	7.07±0.83	6.97±0.76	0.712
Data are mean±standard deviation.			

Table 2. Relative area exposed to shear stress <1 or >7.

	ArterioSorb (n=15) median (IQR)	XIENCE (n=10) median (IQR)	*p*-value
ESS <1 Pa	26.5% (23.5, 42.8)	24.3% (17.4, 26.9)	0.080
ESS >7 Pa	3.4% (0.2, 4.3)	1.3% (0.5, 2.9)	0.285
Values are expressed as percent lumen area exposed to low (<1) or high ESS (>7)[16]. ESS: endothelial shear stress; IQR: interquartile range			

STRUT PROTRUSION AND SHEAR STRESS

Mean strut protrusion was higher in ArterioSorb than in XIENCE (72.6±10.2 vs 42.6±13.7 µm, difference 29.9 µm [95% confidence interval: 27.1 to 32.8], p<0.001). The relationship between strut protrusion and ESS is shown in **Figure 3**. A significant linear relationship was observed between strut protrusion and relative area with shear stress <1 Pa (plotted per cross-section) in ArterioSorb but not in XIENCE. An exponential curve [thick grey line, y=(5.3e-3)*exp(4.2e-2*x) + 0.19, R^2=0.130] was fitted for the overall population, suggesting that strut protrusion of less than 60 µm does not affect shear stress.

Discussion

The main findings of this study are the following. 1) QCA analysis demonstrated similar mean and minimal lumen diameters post procedure in ArterioSorb and XIENCE. Recoil profiles in ArterioSorb after device implantation and after post-dilatation matched those of XIENCE. 2) Post-procedural OCT confirmed similar post-procedural luminal and device dimensions in the two groups. 3) CFD analysis demonstrated comparative ESS between the two devices.

This oriented polylactide polymer rendered the manufacture of thinner struts possible without loss of radial force and without increase in recoil. Acute recoil analysis by QCA in comparison with XIENCE using the same animal indicates that the recoil post implantation or post-dilatation is comparable.

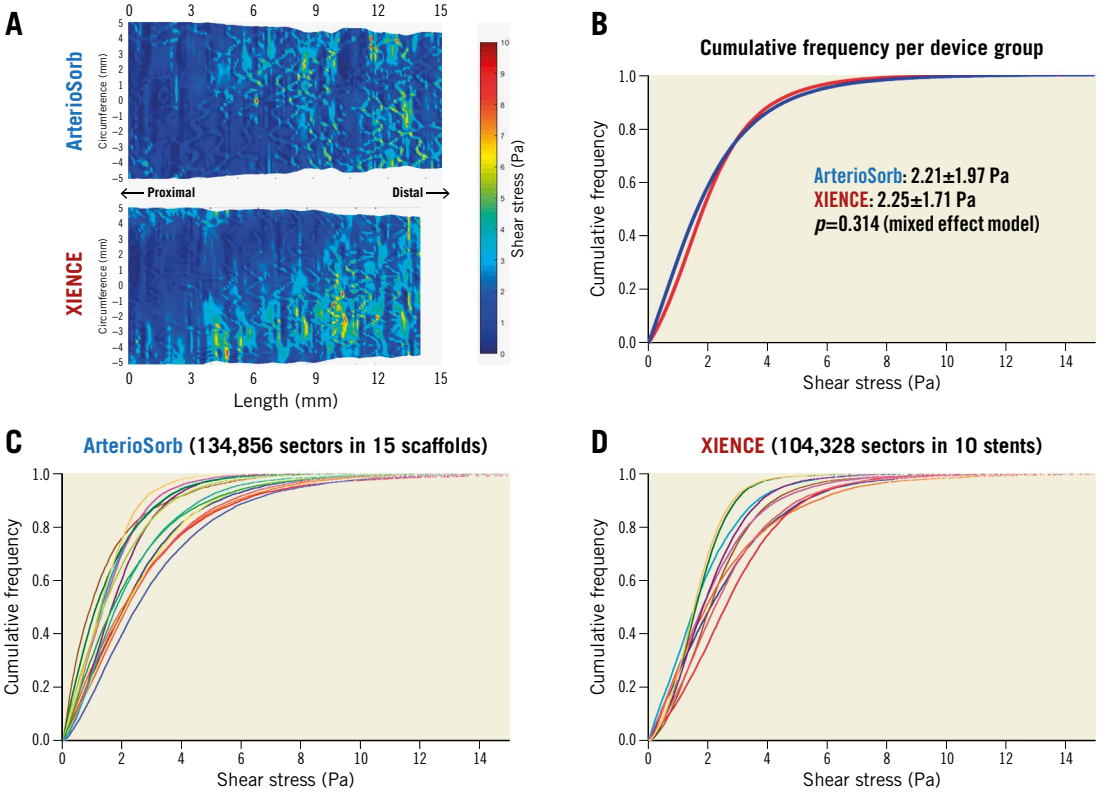

Figure 2. *Comparison of shear stress in the ArterioSorb BRS and XIENCE DES. A) Spread-out maps of representative cases in ArterioSorb (above) and XIENCE (bottom). B), C) & D) Cumulative frequency curves of ESS values in five-degree sectors per device group, each case in ArterioSorb, and each case in XIENCE, respectively. Note that the cumulative frequency curves per device group were almost superimposed. BRS: bioresorbable scaffold; DES: drug-eluting stent*

Previous studies showed that thick BRS struts result in low ESS of the device segment[13]. Thin struts protrude less in the lumen and create fewer low ESS regions that are known to trigger and promote neointimal hyperplasia and neoatherosclerosis[7,14]. In the present study, ArterioSorb, with its reduced strut thickness of 95 µm, close to that of the XIENCE (89 µm), demonstrated comparative ESS to the XIENCE device. While there was a non-significant increase in the relative area exposed to low ESS (<1 Pa) in ArterioSorb as compared to XIENCE in the present analysis, a previous *in vitro* experiment suggested there is no significant difference in thrombogenicity between the 95 µm ArterioSorb and the XIENCE, whereas thrombogenicity in 150 µm BRS was significantly higher than in these two devices[15].

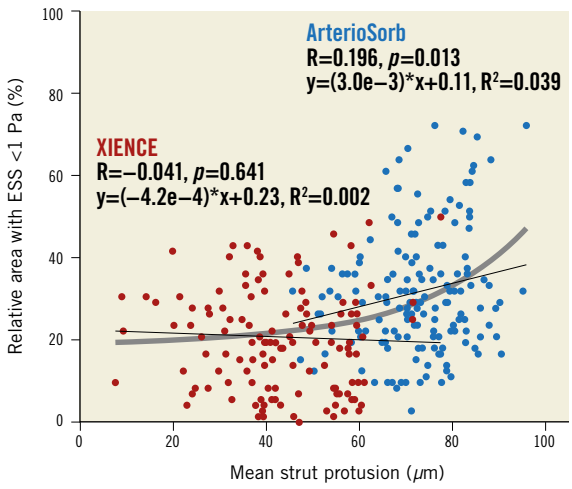

Figure 3. *Relationships between strut protrusion and relative area with low shear stress. ESS: endothelial shear stress*

Our analysis showed that strut protrusion below a threshold of 60 µm does not affect shear stress **(Figure 3)**. If the thickness of a strut came close to 60 µm, there would be no significant differences in the shear stress distribution amongst devices.

Following the present study showing comparative mechanical performance and CFD results of the ArterioSorb BRS as compared to the XIENCE DES, planning of a first-in-man trial is underway.

Study limitations

This is an acute phase study demonstrating the acute performance of a novel bioresorbable scaffold. Follow-up evaluation by QCA, OCT and histology will unravel the device behaviour over time. Further preclinical evaluation will be required to assess mechanical behaviour and resorption profile. The study was performed in a non-atherosclerotic porcine model; therefore, the effect of atherosclerosis on the performance of the device cannot be assessed.

Conclusions

Using oriented PLLA, radial strength is considerably increased and thin struts of 95 µm are made possible. In a porcine model, ArterioSorb scaffolds demonstrated comparable luminal dimensions and shear stress post procedure in comparison with XIENCE best-in-class DES.

Impact on daily practice

A thin-strut bioresorbable scaffold with oriented PLLA is expected to have better mechanical properties than conventional PLLA scaffolds, and equivalent ones to metallic DES. Using oriented PLLA, the radial strength of the 95 µm ArterioSorb BRS was considerably increased and equal to the XIENCE DES, resulting in comparable QCA and OCT results as well as similar endothelial shear stress.

Guest Editor

This paper was guest edited by Alec Vahanian, MD, PhD; Department of Cardiology, Hôpital Bichat-Claude Bernard, and University Paris VII, Paris, France.

Funding

This study was funded by Arterius Ltd, Leeds, United Kingdom. M. Tomaniak acknowledges funding received from the European Society of Cardiology in the form of an ESC 2018 grant.

Conflict of interest statement

J.J. Piek receives non-financial support (travel costs for meetings and educational symposia) from Abbott Vascular as a former member of the medical advisory board. N. Bullett is an operations manager at Arterius Ltd. N. Ahmed is a development scientist at Arterius Ltd. K. Al-Lamee is a CEO/CTO at Arterius Ltd. G. Leclerc is a shareholder of AccelLAB Inc. P.W. Serruys reports consultancy fees from Abbott, Biosensors, Medtronic, Micell, Qualimed, Sinomedical Sciences, St. Jude Medical, Stentys, Svelte Medical Systems, Philips/Volcano, Xeltis, StentIt and HeartFlow. The other authors have no conflicts of interest to declare. The Guest Editor is a consultant for Edwards Lifesciences.

References

1. Ali ZA, Gao RF, Kimura T, Onuma Y, Kereiakes DJ, Ellis SG, Chevalier B, Vu MT, Zhang Z, Simonton CA, Serruys PW, Stone GW. Three-Year Outcomes With the Absorb Bioresorbable Scaffold: Individual-Patient-Data Meta-Analysis From the ABSORB Randomized Trials. *Circulation.* 2018;137:464-79.

2. Guidance for industry and FDA staff: non-clinical engineering tests and recommended labelling for intravascular stents and associated delivery systems. http://www.fda.gov/MedicalDevices/DeviceRegulationandGuidance/GuidanceDocuments/ucm071863.htm. [Last accessed on 11 Oct 2018].

3. Onuma Y, Serruys PW, Gomez J, de Bruyne B, Dudek D, Thuesen L, Smits P, Chevalier B, McClean D, Koolen J, Windecker S, Whitbourn R, Meredith I, Garcia-Garcia H, Ormiston JA; ABSORB Cohort A and B investigators. Comparison of in vivo acute stent recoil between the bioresorbable everolimus-eluting coronary scaffolds (revision 1.0 and 1.1) and the metallic everolimus-eluting stent. *Catheter Cardiovasc Interv.* 2011;78:3-12.

4. Nakatani S, Sotomi Y, Ishibashi Y, Grundeken MJ, Tateishi H, Tenekecioglu E, Zeng Y, Suwannasom P, Regar E, Radu MD, Räber L, Bezerra H, Costa MA, Fitzgerald P, Prati F, Costa RA, Dijkstra J, Kimura T, Kozuma K, Tanabe K, Akasaka T, Di Mario C, Serruys PW, Onuma Y. Comparative analysis method of permanent metallic stents (XIENCE) and bioresorbable poly-L-lactic (PLLA) scaffolds (Absorb) on optical coherence tomography at baseline and follow-up. *EuroIntervention.* 2016;12:1498-509.

5. Sotomi Y, Tateishi H, Suwannasom P, Dijkstra J, Eggermont J, Liu S, Tenekecioglu E, Zheng Y, Abdelghani M, Cavalcante R, de Winter RJ, Wykrzykowska JJ, Onuma Y, Serruys PW, Kimura T. Quantitative assessment of the stent/scaffold strut embedment analysis by optical coherence tomography. *Int J Cardiovasc Imaging.* 2016;32:871-83.

6. Bourantas CV, Papafaklis MI, Athanasiou L, Kalatzis FG, Naka KK, Siogkas PK, Takahashi S, Saito S, Fotiadis DI, Feldman CL, Stone PH, Michalis LK. A new methodology for accurate 3-dimensional coronary artery reconstruction using routine intravascular ultrasound and angiographic data: implications for widespread assessment of endothelial shear stress in humans. *EuroIntervention.* 2013;9:582-93.

7. Bourantas CV, Papafaklis MI, Kotsia A, Farooq V, Muramatsu T, Gomez-Lara J, Zhang YJ, Iqbal J, Kalatzis FG, Naka KK, Fotiadis DI, Dorange C, Wang J, Rapoza R, Garcia-Garcia HM, Onuma Y, Michalis LK, Serruys PW. Effect of the endothelial shear stress patterns on neointimal proliferation following drug-eluting bioresorbable vascular scaffold implantation: an optical coherence tomography study. *JACC Cardiovasc Interv.* 2014;7:315-24.

8. Manbachi A, Hoi Y, Wasserman BA, Lakatta EG, Steinman DA. On the shape of the common carotid artery with implications for blood velocity profiles. *Physiol Meas*. 2011;32:1885-97.

9. Popel AS, Enden G. An analytical solution for steady flow of a Quemada fluid in a circular tube. *Rheol Acta*. 1993;32:422-6.

10. Poon EKW, Thondapu V, Hayat U, Barlis P, Yap CY, Kuo PH, Wang Q, Ma J, Zhu SJ, Moore S, Ooi ASH. Elevated Blood Viscosity and Microrecirculation Resulting From Coronary Stent Malapposition. *J Biomech Eng.* 2018 May 1;140(5).

11. van der Giessen AG, Groen HC, Doriot PA, de Feyter PJ, van der Steen AF, van de Vosse FN, Wentzel JJ, Gijsen FJ. The influence of boundary conditions on wall shear stress distribution in patients specific coronary trees. *J Biomech.* 2011;44:1089-95.

12. Siasos G, Sara JD, Zaromytidou M, Park KH, Coskun AU, Lerman LO, Oikonomou E, Maynard CC, Fotiadis D, Stefanou K, Papafaklis M, Michalis L, Feldman C, Lerman A, Stone PH. Local Low Shear Stress and Endothelial Dysfunction in Patients With Nonobstructive Coronary Atherosclerosis. *J Am Coll Cardiol.* 2018;71:2092-102.

13. Tenekecioglu E, Sotomi Y, Torii R, Bourantas C, Miyazaki Y, Collet C, Crake T, Su S, Onuma Y, Serruys PW. Strut protrusion and shape impact on endothelial shear stress: insights from pre-clinical study comparing Mirage and Absorb bioresorbable scaffolds. *Int J Cardiovasc Imaging.* 2017;33:1313-22.

14. Torii R, Stettler R, Räber L, Zhang YJ, Karanasos A, Dijkstra J, Patel K, Crake T, Hamshere S, Garcia-Garcia HM, Tenekecioglu E, Ozkor M, Baumbach A, Windecker S, Serruys PW, Regar E, Mathur A, Bourantas CV. Implications of the local hemodynamic forces on the formation and destabilization of neoatherosclerotic lesions. *Int J Cardiol.* 2018;272:7-12.

15. Lu S, Ng J, Ang H, Paradies V, Wong PE, Al-Lamee R, Al-Lamee K, Bullett N, Ahmed N, Joner M, Foin N. Is There Light at the End of the Thin-Strut Tunnel?: In Vitro Insights on Strut Thickness Impact on Thrombogenicity in Bioresorbable Stents or Scaffolds. *JACC Cardiovasc Interv.* 2018;11:714-6.

16. Malek AM, Alper SL, Izumo S. Hemodynamic shear stress and its role in atherosclerosis. *JAMA.* 1999;282:2035-42.

Supplementary data

Supplementary Appendix 1. *In vitro* radial strength testing.

Supplementary Appendix 2. Angiogram acquisition and QCA analysis.

Supplementary Appendix 3. Shear stress analysis.

Supplementary Appendix 4. Statistical analysis.

Supplementary Figure 1. ArterioSorb scaffold utilising oriented PLLA technology.

Supplementary Figure 2. Radial strength test providing a "diameter vs force" curve.

Supplementary Figure 3. Radial strength testing of ArterioSorb.

Supplementary Figure 4. Flow chart showing feasibility of shear stress analysis.

Supplementary Table 1. Procedural characteristics in preclinical porcine study.

Supplementary Table 2. Results of quantitative coronary angiography.

The supplementary data are published online at: https://eurointervention.pcronline.com/doi/10.4244/EIJ-D-18-01190

Supplementary data

Supplementary Appendix 1. In vitro radial strength testing

Radial force of the expanded ArterioSorb scaffolds was assessed using the RX550 (Machine Solutions Inc., Flagstaff, AZ, USA) by imposing a circumferentially uniform radial load reducing the scaffold diameter by 50%. The ArterioSorb scaffolds were 3.0 or 3.5 x 14 mm while a control sample of XIENCE 3.0 x 18 mm was measured in the same way. The temperature of RX550 was set to 37±2°C. The radial force and the diameter were recorded while decreasing the scaffold diameter. The measured forces were normalised for stent length to allow direct comparison.

For each sample group, three scaffolds were tested, except for the XIENCE control, where only one sample was available. The radial strength test provided a curve of diameter versus force **(Supplementary Figure 2)**. Each curve consisted of a linear increase in constrictive force with reduction in diameter, followed by an inflexion point where permanent deformation of the scaffold/stent occurred (radial force at inflexion point). Afterwards, the force required to compress the scaffold/stent increased until 50% diameter compression was reached (maximum radial force). This resulted in a destructive test with sudden collapse of the device that was outside of the normal operating range of the scaffolds. The linear region of force versus diameter was used to calculate the stiffness until inflexion point, which was the radial stiffness until the buckling point. After this, the scaffolds lost stiffness as they were not able to resist the compressive forces [2].

The results of the radial force assessments are shown in **Supplementary Figure 3**. The maximum radial forces of ArterioSorb scaffolds were marginally higher than XIENCE. The ArterioSorb scaffolds had significantly higher radial force at inflexion point as well as stiffness until inflexion point than the XIENCE.

Supplementary Appendix 2. Angiogram acquisition and QCA analysis

After administering nitroglycerine, coronary angiography was performed. When there were multiple projections at a single time point, the fluoroscopic image with the minimal foreshortening was selected.

Quantitative coronary angiography (QCA) measurements were performed using CAAS 5.11.2 (Pie Medical Imaging B.V., Maastricht, the Netherlands). The mean and minimal lumen diameters were measured before the procedure, after device implantation, and post procedure. Additionally, mean and minimal diameters of the inflated balloon at maximum pressure were measured during scaffold/stent implantation and during post-dilation. Balloon to artery ratios were based on mean balloon and preprocedural lumen diameter.

Acute recoil was evaluated using mean lumen diameter after device implantation or at the end of procedure and related to the mean balloon diameter at the previous sequence [3]. Global recoil was defined as the difference in lumen diameter between at device implantation and at the end of the procedure.

OCT acquisition and analysis

Optical coherence tomography (OCT) was performed pre- and post-procedure using the ILUMIEN™ Optis™ imaging system (Abbott Vascular, Santa Clara, CA, USA). Nitroglycerine was delivered to achieve vasodilatation prior to performing the OCT pullback.

The OCT recordings were analysed using QCU-CMS software, version 4.7 (Medis, Leiden, the Netherlands). Taking into account the difference in the optical properties of polylactide and CoCr, OCT analysis was performed using comparative methods previously described by our core lab [4]. Strut protrusion and embedment were quantified using a validated method [5]. Quantitative assessment of OCT was performed at 1 mm intervals.

Both QCA and OCT analyses were performed by an independent core laboratory (Cardialysis BV, Rotterdam, the Netherlands).

Supplementary Appendix 3. Shear stress analysis

Three-dimensional reconstruction of the coronary artery

Three-dimensional (3D) model reconstruction of the coronary artery was based on a 3D centreline derived from 3D QCA of the vessel implanted with the device and co-registration of the flow area contour of OCT onto the 3D centreline [6].

Three-dimensional QCA was performed using QAngioXA 3D, version 1.3 (Medis, Leiden, the Netherlands). Two post-procedural end-diastolic angiographic images with at least 25º-

angle difference with minimal foreshortening were selected and analysed. The luminal centreline derived from 3D QCA was extracted.

OCT images were analysed throughout the entire pullback. Flow area segmentation was performed at 100 μm intervals in the device segment and 400 μm intervals in the native vessel segments [7]. The flow area was traced and defined in the native segments by the luminal border and in the device segments by the endoluminal side of the struts and by the vessel luminal surface borders between the struts.

The borders of flow area identified on OCT images were placed perpendicularly onto the 3D centreline using anatomical landmarks (i.e., side branches) and the radiopaque markers or stent edges identified both on angiography and OCT (3D IVUS/OCT registration; Medis, Leiden, the Netherlands) [6]. OCT cross-sections were placed as long as possible, in order to adjust for the effect of proximal swirling flow induced by vessel curvature [8] as much as possible.

The proximal side branch (SB) (>1.0 mm in diameter) closest to the device was modelled in 3D QCA and included in the 3D model, regardless of the distance from the proximal edge of the device to the SB in order to account for the effect of flow division and the effect of any flow disturbance caused by the carina zone of the SB. SB (>1.0 mm in diameter) within the device segment was also included in the model.

Computational fluid dynamics analysis

The reconstructed 3D coronary artery models were meshed with small tetrahedral cells for computational fluid dynamics (CFD), using ANSYS ICEM CFD 17.1 (ANSYS, Inc., Canonsburg, PA, USA). Three prism layers at the wall were added. In order to incorporate its shear-thinning behaviour, blood was modelled as a non-Newtonian fluid by applying the Quemada equation [9]. The Quemada equation depends on both shear rate and haematocrit (Hct)

$$\mu = \left(\sqrt{\mu_\infty} + \frac{\sqrt{\tau_0}}{\sqrt{\lambda} + \sqrt{\dot{\gamma}}}\right)^2$$

and its coefficients were assumed as 45% Hct and a constant blood density of 1,060 $kg \cdot m^{-3}$, τ_0=7.16×10^{-3} Pa, μ_∞= 4.204×10^{-3} Pa·s, and λ=4.367×10^{-3} s^{-1} [10]. The vessel wall was

modelled as rigid and a no-slip condition was imposed at the wall. For the outflow conditions in the main vessel and side branches, flow rates were estimated based on the vessel diameters, following the relationship derived from *in vivo* observations (scaling approach) [11]. Coronary blood flow at the inlet was estimated by frame count and travel distance of the contrast agent in the X-ray angiogram [12]. A finite volume solver was used to perform steady-state blood flow simulations using standard numerical techniques (ANSYS Fluent v17.1; ANSYS, Inc. Canonsburg, PA, USA).

In post-processing of the CFD result, the ESS was extracted at the location of each OCT frame along the lumen centreline using an in-house program in MATLAB (MathWorks, Natick, MA, USA). ESS in each five-degree sector along the circumference at every OCT frame was measured for statistical analysis [13].

Supplementary Appendix 4. Statistical analysis

Binary variables were presented as counts and percentages and compared using Pearson's chi-squared test or Fisher's exact test, as appropriate. Continuous variables were presented as mean and standard deviation or median with interquartile range (IQR) and compared using the Student's t-test or Mann-Whitney U test, as appropriate. ESS in five-degree sectors in cross-section were compared between devices using a linear mixed model to take into account the clustering nature of the sectors within cross-section within device. The relationship between strut protrusion and ESS was explored using linear regression and Pearson's correlation coefficient [13]. A p-value <0.05 was considered statistically significant. All statistical analyses were performed using SPSS, Version 24.0.0.2 (IBM Corp., Armonk, NY, USA).

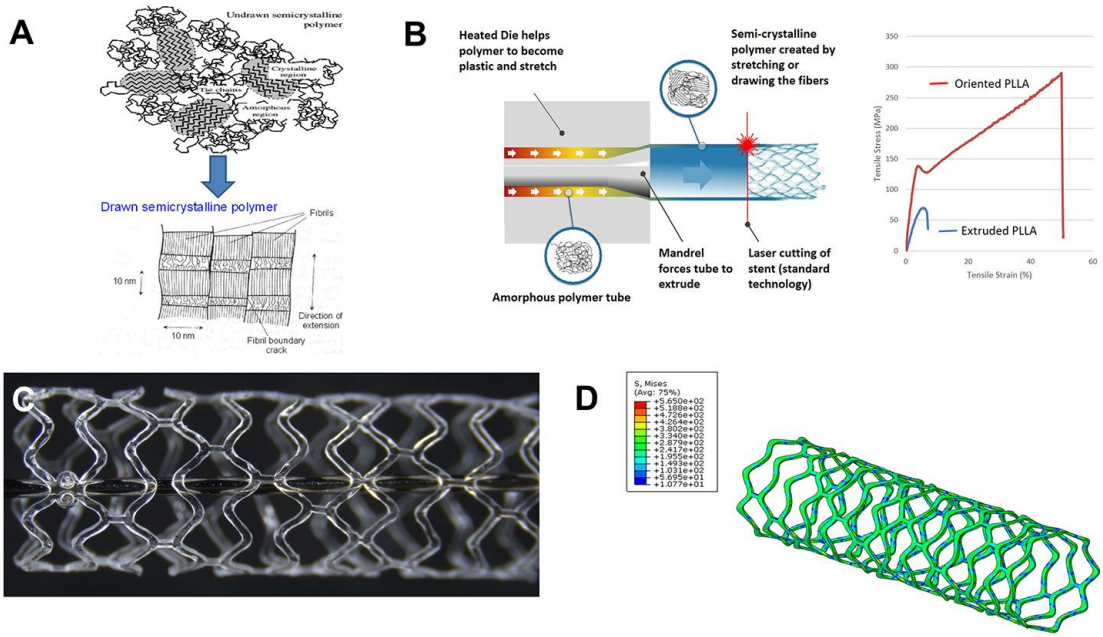

Supplementary Figure 1. ArterioSorb scaffold utilising oriented PLLA technology. Semi-crystalline polymer is processed and drawn into a highly oriented form (A). The heated die helps polymer to become plastic and stretched and the mandrel forces the polymeric tubes for extrusion. At the end of extrusion, semi-crystalline polymer is created by stretching and/or drawing the fibres. Oriented PLLA provides much higher tensile strength compared to the extruded PLLA (B). The design of the spiral connectors provides high radial strength and appropriate flexibility for ease of implantation (C). The finite element method provides mechanical analysis of the stent/scaffolds; the contour maps of von Mises stress in the ArterioSorb demonstrated not so severe stress concentrations at the peaks of the strut rings which potentially denotes lower risk of fracture during deployment (D).

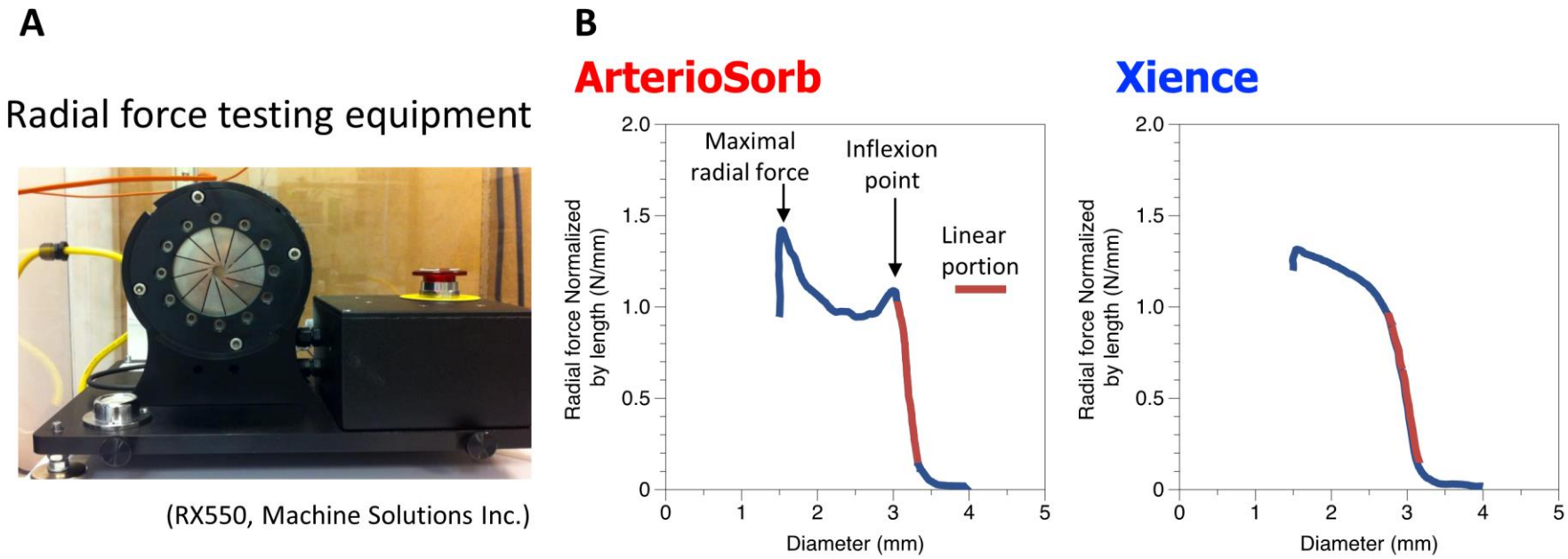

Supplementary Figure 2. Radial strength test providing a "diameter vs force" curve.

A) The equipment used for radial force testing (RX550; Machine Solutions Inc., Flagstaff, AZ, USA).

B) Diameter vs radial force curves of the ArterioSorb (left) and the XIENCE (right). A curve consisted of a linear increase in constrictive force with reduction in diameter, followed by an inflexion point where permanent deformation of the scaffold/stent occurred (radial force at inflexion point). Afterwards, the force required to compress the scaffold/stent increased until 50% diameter compression was reached (maximum radial force). The linear region of force versus diameter was used to calculate the stiffness until inflexion point, which was the radial stiffness until the buckling point.

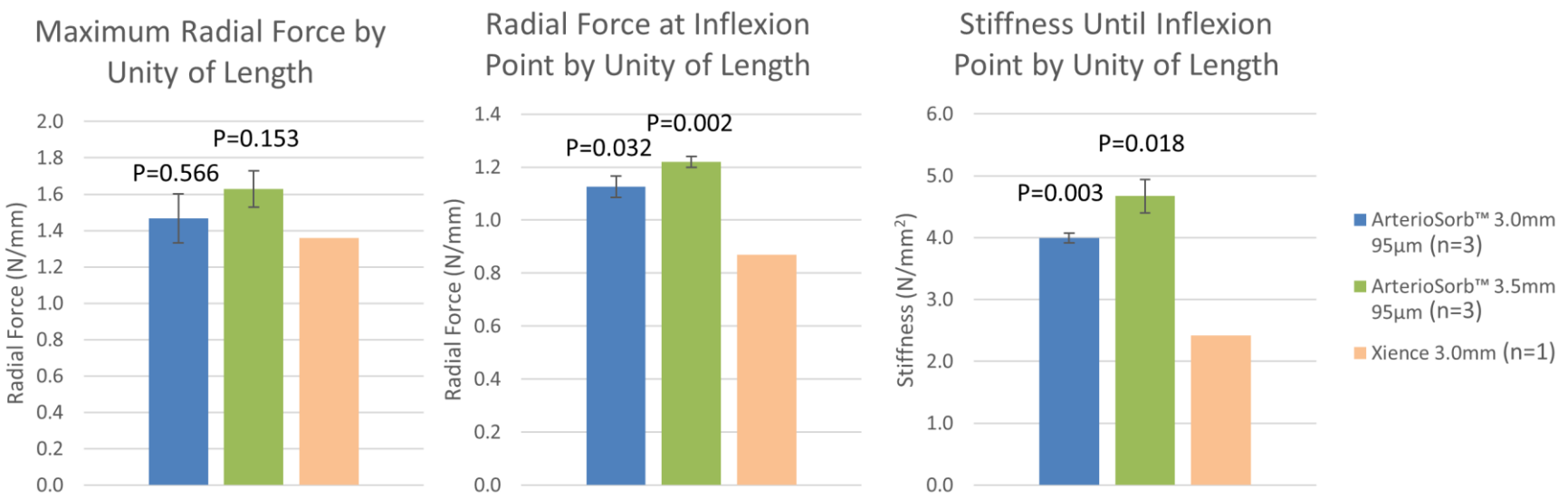

Supplementary Figure 3. Radial strength testing of the ArterioSorb.

Left panel: maximum radial force; middle panel: radial force at inflexion point; right panel: stiffness until inflexion point. P-values are against the XIENCE.

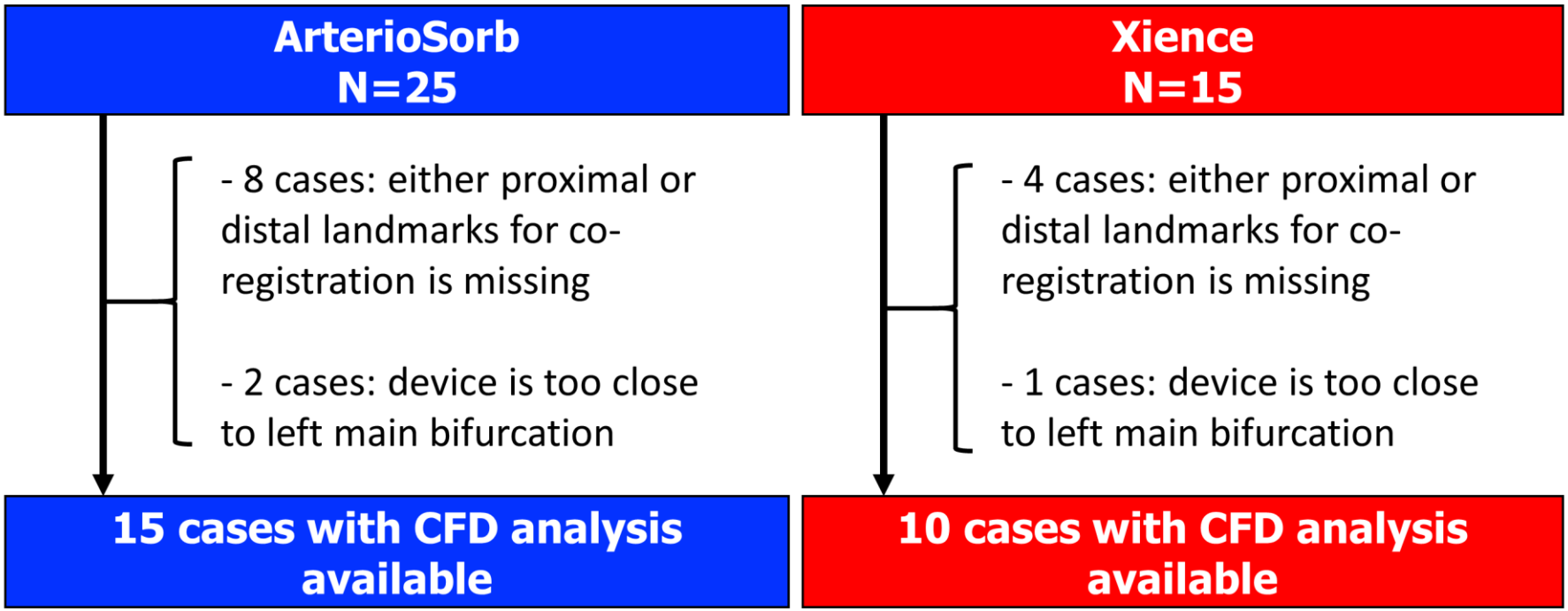

Supplementary Figure 4. Flow chart showing feasibility of shear stress analysis.

CFD: computational fluid dynamics

Supplementary Table 1. Procedural characteristics in preclinical porcine study.

	ArterioSorb (n=25)	XIENCE (n=15)	*p*-value
Vessel			0.159
Right coronary artery	15 (60.0)	6 (40.0)	
Left anterior descending artery	6 (24.0)	8 (53.3)	
Left circumflex artery	4 (16.0)	1 (6.7)	
Nominal diameter of device, mm	3.0	3.0	NA
Nominal length of device, mm	14	15	NA
Maximal pressure during device implantation, atm	14.04±3.01	12.40±3.74	0.136
Post-dilatation performed	25 (100.0)	12 (80.0)	0.046
Nominal diameter of post-dilatation balloon, mm	3.16±0.12	3.10±0.13	0.210
Maximal pressure during post-dilatation, atm	19.24±4.80	18.42±4.56	0.623

Data are count (percentage) or mean±standard deviation.

Supplementary Table 2. Results of quantitative coronary angiography.

	ArterioSorb (n=25)	XIENCE (n=15)	*p*-value
Pre-procedure			
Mean lumen diameter, mm	2.79±0.28	2.72±0.30	0.450
Minimum lumen diameter, mm	2.55±0.31	2.49±0.28	0.507
Device balloon			
Mean diameter, mm	3.01±0.27	3.02±0.19	0.932
Minimum lumen diameter, mm	2.83±0.28	2.81±0.23	0.824
Device balloon-artery ratio	1.09±0.11	1.12±0.11	0.335
Immediately after device deployment			
Mean lumen diameter, mm	2.87±0.30	2.94±0.17	0.458
Minimum lumen diameter, mm	2.59±0.31	2.65±0.25	0.551
Absolute recoil after device deployment, mm	0.14±0.22	0.09±0.15	0.388
Relative recoil after device deployment, %	4.69±7.38	2.70±4.52	0.367
Post-dilatation balloon (segment in device)			
Mean diameter, mm	3.07±0.20	3.10±0.14	0.689
Minimum lumen diameter, mm	2.92±0.23	2.94±0.14	0.766
Post-dilatation balloon-artery ratio	1.11±0.09	1.14±0.10	0.385
Post-procedure			
Mean lumen diameter, mm	2.98±0.19	3.01±0.16	0.564
Minimum lumen diameter, mm	2.79±0.21	2.76±0.18	0.634
Absolute recoil from post-dilatation to post-procedure, mm	0.09±0.17	0.10±0.16	0.931
Relative recoil from post-dilatation to post-procedure, %	2.81±5.52	3.03±5.21	0.907
Global recoil from device implantation to post-procedure (only device with post-dilatation)			
Absolute global recoil, mm	0.03±0.27	-0.01±0.18	0.636
Relative global recoil, %	0.55±8.27	-0.46±5.64	0.705

Data are mean±standard deviation.